Journal of Sound and Vibration (1998) **212**(4), 623–635

THE STEELPAN AS A SYSTEM OF NON-LINEAR MODE-LOCALIZED OSCILLATORS, PART III: THE INVERSE PROBLEM—PARAMETER ESTIMATION

A. ACHONG

Department of Physics, University of the West Indies, St. Augustine, Trinidad, West Indies

(*Received* 18 *June* 1997, *and in final form* 17 *November* 1997)

This paper is the third in the series on this topic. In the earlier papers, the dynamics of the steelpan notes were developed as systems of non-linear mode-localized oscillators which can show note–note and note–skirt coupling. The tonal qualities of a note depend on the coupling parameters and damping coefficients. Here, the inverse problem of parameter estimation is presented for notes that do not show coupling to other subsystems of the instrument.

1. INTRODUCTION

In earlier papers [1, 2] (when appropriate, these references may be referred to as Part I and Part II respectively) the physical structure of the steelpan was described and an examination made of the responses of the notes and other subsections to impacts produced by striking the notes with the stick (mallet). Each note was modelled as a non-linear system for which the governing equations for note vibrations contained linear and quadratic terms. Quadratic non-linearities arise from the curvature of the notes, which are formed as shallow shell-like domes on the indented face of a steel drum. The exchange of energy between resonances on a note produces amplitude as well as frequency modulations.

This paper is concerned with the specific inverse problem of estimating the parameters for the analytical model developed for the steelpan in references [1] and [2]. This work should add to the body of knowledge on inverse problems of vibrating systems (see, for example, Lancaster and Maroulas [3], Starek and Inman [4, 5] and the review papers by Gladwell [6, 7]) and to the area of *model updating* (see the survey by Mottershead and Friswell [8]).

2. THEORETICAL DEVELOPMENT

Consider a small element of area dA at some arbitrary position $\mathbf{r}$ on the note. To describe the vibration of such an element, a general deflection function is sought which describes the non-linear modes of the system. To satisfy this requirement, the procedure of references [1] and [2] is followed by defining, for an arbitrary element, a deflection function

$$w(\mathbf{r}, t) = \sum_{n=1}^{\infty} u_n(t) V_n(\mathbf{r}), \tag{1}$$

0022–460X/98/190623 + 13 $25.00/0/sv971458

where $V_n(\mathbf{r})$ are appropriate spatial functions (mode shapes) satisfying the boundary conditions of the note, n is the mode number, and $u_n(t)$ are unknown functions of time only.

As in reference [1], the governing equation for the free vibrations on the steelpan notes can be expressed by

$$\ddot{u}_n + \omega_n^2 u_n + \varepsilon\left[2\mu_n \dot{u}_n - \sum_{j=1}^{\infty}\sum_{k=1}^{\infty} \alpha_{j,k,n}\, u_j\, u_k\right] = 0, \tag{2}$$

where u_n are the displacements; the dots refer to differentiation with respect to t; ω_n are the frequencies of the system with $\omega_1 < \omega_2 < \ldots < \omega_\infty$; μ_n are the damping coefficients; α_{jkn} are constants with $\alpha_{jkn} = \alpha_{kjn}$, and ε is a small gauge parameter. Also as in reference [1], the note is treated as a 3-DOF system in which the second mode ($n = 2$) corresponds to an internal resonance and the third mode ($n = 3$) represents a combination resonance (a heterodyne effect represented by the cross-modal term $\alpha^*_{123}\, u_1\, u_2$). This is a sufficient description, as the fourth and higher modes have been observed on the steelpan to be very low in amplitude and will produce relatively weak interaction products in combination resonances. The curvature of these shallow shell-like notes [9] gives rise to quadratic nature of equation (2).

By using the multi-time scale procedure (Nafeh and Mook [10] and Nafeh [11]) it can be shown, as in reference [1], that the general solution of equation (2) to order ε^0 takes the form $u_{n0} = A_n(t_1)\, e^{i\omega_n t_0} + CC$, where $A_{nd} = \frac{1}{2} a_{nd}\, e^{i\phi_{nd}}$, with a_{nd} and ϕ_{nd} being functions of the slow time t_1 ($t_n = \varepsilon^n t$) and representing the amplitude and phase of the nth Fourier component of the displacement respectively. By combining this solution with the ε^1 solution, it was also shown in reference[1] that the $(a_1, a_2, a_3, \phi_1, \phi_2, \phi_3)$ phase flow is governed by

$$\begin{aligned}
a_1' &= -\mu_1 a_1 + \frac{\alpha^*_{121}}{4\omega_1} a_1 a_2 \sin\gamma_1 + \frac{\alpha^*_{231}}{4\omega_1} a_2 a_3 \sin\gamma_2,\\
a_2' &= -\mu_2 a_2 - \frac{\alpha_{112}}{4\omega_2} a_1^2 \sin\gamma_1 + \frac{\alpha^*_{132}}{4\omega_2} a_1 a_3 \sin\gamma_2,\\
a_3' &= -\mu_3 a_3 - \frac{\alpha^*_{123}}{4\omega_3} a_1 a_2 \sin\gamma_2,\\
\phi_1' &= -\frac{\alpha^*_{121}}{4\omega_1} a_2 \cos\gamma_1 - \frac{\alpha^*_{231}}{4\omega_1}\frac{a_2 a_3}{a_1}\cos\gamma_2,\\
\phi_2' &= -\frac{\alpha_{112}}{4\omega_2}\frac{a_1^2}{a_2}\cos\gamma_1 - \frac{\alpha^*_{132}}{4\omega_2}\frac{a_1 a_3}{a_2}\cos\gamma_2,\\
\phi_3' &= -\frac{\alpha^*_{123}}{4\omega_3}\frac{a_1 a_2}{a_3}\cos\gamma,
\end{aligned} \tag{3a–f}$$

where $\alpha^*_{jkn} = \alpha_{jkn} + \alpha_{kjn}$, the prime denotes $\mathrm{d}/\mathrm{d}t_1$, and

$$\gamma_1 = \phi_2 - 2\phi_1 + \sigma_1 t_1, \qquad \gamma_2 = \phi_3 - \phi_2 - \phi_1 + \sigma_2 t_1, \tag{4}$$

with the detuning parameters σ_1 and σ_2 describing the closeness of the resonant frequencies:

$$\omega_2 = 2\omega_1 + \varepsilon\sigma_1, \qquad \omega_3 = \omega_1 + \omega_2 + \varepsilon\sigma_2. \tag{5}$$

The parameters $\omega_n, \mu_n, \sigma_1, \sigma_2$ and α_{jkn} allow the full range of frequency- and amplitude-modulation features observed on a steelpan to be modelled mathematically. A practically feasible procedure is therefore sought that may yield those parameters from the time-history data of individual notes. This is *the inverse problem*.

2.1. PHASE FLOW

After some algebraic manipulations of equations (3a–c) to eliminate the sines, one arrives at the equation

$$\tfrac{1}{2}\frac{\mathrm{d}}{\mathrm{d}t_1}[a_1^2 + v_2\, a_2^2 + v_3\, a_3^2] = -[\mu_1\, a_1^2 + \mu_2\, v_2\, a_2^2 + \mu_3 v_3\, a_3^2]. \tag{6}$$

where

$$v_2 = \frac{\omega_2}{\omega_1}\frac{\alpha^*_{121}}{\alpha_{112}}, \qquad v_3 = \frac{\omega_3}{\omega_1}\left(\frac{\alpha^*_{132}\,\alpha^*_{121}}{\alpha^*_{123}\,\alpha_{112}} + \frac{\alpha^*_{231}}{\alpha^*_{123}}\right). \tag{7}$$

A two-mode version of equation (6) has been discussed by Sethna [12]. It is not possible to obtain a complete general solution to equation (6) for the case $\mu_1 \neq \mu_2 \neq \mu_3$. However, a reasonable simplification is to assume equal damping for the three modes; i.e., $\mu_1 = \mu_2 = \mu_3 \overset{\text{def}}{=} \mu$. This assumption is justified by the following consideration. Damping in metals at low stress levels is due primarily to magnetoelastic hysteresis which, in the present frequency range of interest, is independent of frequency [13]. The steel used in the manufacture of steelpans exhibits little internal damping because of the low stress levels involved during a vibration cycle. Acoustic radiation and energy exchanges across the note edges also affect the damping.

The first modes for the notes on the steelpans are all located in the frequency range 69·3 Hz ($C_2^{\#}$) on the low end, to 1396·9 Hz (F_6) on the high end. For the most part, it is only the first three modes of vibration on each note that are of sufficient amplitude to be of significant musical interest. On any particular note therefore, the frequenct range over which the damping is required is somewhat limited. Observation of many steelpan tones shows that the duration of these tones are all of the order of one second. While this latter observation, taken alone, cannot accurately define the damping coefficients for this non-linear instrument, it does imply that the degree of damping is not expected to be highly variable over the frequency range of the instrument.

With the equal damping assumption, equation (6) can be integrated to give

$$E(\tau) = E(0)\,\mathrm{e}^{-2\mu\tau}, \tag{8}$$

where

$$E(\tau) = a_1^2 + v_2\, a_2^2 + v_3\, a_3^2 \tag{9}$$

and τ (in units of the time scale t_1) is the time measured from the instant that E maximizes. The latter occurs some time after the stick has lost contact with the note.

Were the damping coefficients of the second and third modes to be written as $\mu_2 = \mu_1 + \delta\mu_2$, $\mu_3 = \mu_1 + \delta\mu_3$, to account for differences in damping coefficients, then equation (8) would have to be replaced by

$$E(\tau) = E(0)\,\mathrm{e}^{-2[\mu_1\,\tau\, +\, g(\tau)]}$$

with

$$g(\tau) = \int_0^\tau \frac{\delta\mu_2\, v_2\, a_2^2 + \delta\mu_3\, v_3\, a_3^2}{a_1^2 + v_2\, a_2^2 + v_3\, a_3^2}\,\mathrm{d}\tau', \tag{10a, b}$$

where τ' is a dummy time variable over the interval $[0, \tau]$. If $\delta\mu_2$ and $\delta\mu_3$ are significantly

different from zero, then $E(\tau)$ will not follow an exponential law. It ought to be possible to test, empirically, the applicability of these equations to the steelpan notes.

From equations (8) and (9),

$$\frac{a_1^2}{B_1} + \frac{a_2^2}{B_2} + \frac{a_3^2}{B_3} = \mathrm{e}^{-2\mu\tau}, \tag{11}$$

where

$$B_1 = E(0), \qquad B_2 = \frac{E(0)}{\nu_2}, \qquad B_3 = \frac{E(0)}{\nu_3}. \tag{12a–c}$$

Equation (11) shows that, under equal damping, the modal amplitudes a_n are not independent of each other, but that a weighted sum of the squares of the modal amplitudes should follow an exponential decay law. For a conservative system ($\mu = 0$), the solutions lie on an ellipsoid in the six-dimensional phase space ($a_1, a_2, a_3, \phi_1, \phi_2, \phi_3$). For a dissipative system, however, such as the notes on the steelpan, this ellipsoid slowly collapses as the tone decays.

From an energy standpoint, equation (11) describes the partition of energy amongst the three modes.

2.2. FREQUENCY–AMPLITUDE RELATION

Equations (3d–f) can be reduced to

$$\phi_1' a_1^2(\tau) - \frac{\omega_2}{\omega_1}\frac{\alpha_{121}^*}{\alpha_{112}}\phi_2' a_2^2(\tau) - \frac{\omega_3}{\omega_1}\left[\frac{\alpha_{231}^*}{\alpha_{123}^*} - \frac{\alpha_{132}^*\,\alpha_{121}^*}{\alpha_{123}^*\,\alpha_{112}}\right]\phi_3' a_3^2(\tau) = 0. \tag{13}$$

Equation (13) shows the relationship of the frequency modulations ϕ_n' to the amplitudes $a_n(\tau)$. Examples of this frequency-amplitude dependence as found on the steelpan, were given in the experimental and numerical data of reference [1].

2.3. SOLUTION TO THE INVERSE PROBLEM

Before proceeding with the inverse problem, the observation data are defined.

2.3.1. *Observation data*

The data provided by observation of the steelpan are in the form of displacement (or velocity) time histories of the vibrating notes. The notes are set into vibration by impact using a standard rubber-tipped stick. Velocity measurements can be made using a set-up consisting of a small electrodynamic velocity tranducer, low-noise amplifier, anti-aliasing filter, A/D converter and a desktop computer. This raw data can be analyzed using the Short-Time-Fourier-Transform (STFT) (discussed fully in Part I) to produce complex spectral components $S_{\dot{u}}^{\{n\}}$ for the velocity $\dot{u}$. These velocity STFT components are linearly related to the STFT $S_u^{\{n\}}$ for displacement u by, $S_{\dot{u}}^{\{n\}} = -\mathrm{j}\omega_n S_u^{\{n\}}$. In the present analysis, there exists the correspondence $a_n \equiv |S_u^{\{n\}}|$, $\phi_n \equiv \arg(S_u^{\{n\}})$. The inverse problem based on this correspondence is given below.

2.3.2. *Inverse parameter value problem*

Given the observation data in the above form, determine the values of $(\omega_n, \mu_n, \sigma_1, \sigma_2, \alpha_{jkn})$.

Remark. An obvious question that arises is that of the uniqueness of $(\omega_n, \mu_n, \sigma_1, \sigma_2, \alpha_{jkn})$ recovered from the observation data.

To see more clearly what parameters can be determined, equation (10) must be written in the more explicit form

$$a_1^2(\tau) - a_1^2(0)\,\mathrm{e}^{-2[\mu_1\tau + g(\tau)]} + \frac{\omega_2}{\omega_1}\frac{\alpha^*_{121}}{\alpha_{112}}[a_2^2(\tau) - a_2^2(0)\,\mathrm{e}^{-2[\mu_1\tau + g(\tau)]}]$$

$$+\frac{\omega_3}{\omega_1}\left(\frac{\alpha^*_{231}}{\alpha^*_{123}} + \frac{\alpha^*_{132}\,\alpha^*_{121}}{\alpha^*_{123}\,\alpha_{112}}\right)[a_3^2(\tau) - a_3^2(0)\,\mathrm{e}^{-2[\mu_1\tau + g(\tau)]}] = 0. \tag{14}$$

From equations (13) and (14), one sees that the α parameters cannot be determined individually but only in the combined form of ratios $\alpha^*_{121}/\alpha_{112}$, $\alpha^*_{132}/\alpha^*_{123}$ and $\alpha^*_{231}/\alpha^*_{123}$. This, at least partially, answers the question on the uniqueness of the α parameters.

The use of the slow time τ $(=\varepsilon t)$ in equation (14) means that in practice, where it is the real time (or fast time) t that is measurable, only the products $\varepsilon\mu_n$ can be determined from the experimental data. Similarly, for the detuning parameters, only the products $\varepsilon\sigma_n$ can be determined.

The frequencies ω_n (and frequency modulations) are easily recovered by maximizing the STFT's as described fully in Part I and Part II. These frequency values will be unique for each note.

2.3.3. *Minimization and discretization*

Values for $\varepsilon\mu_n$, $(\omega_2/\omega_1)/(\alpha_{112}/\alpha^*_{121})$ and $(\omega_3/\omega_1)(\alpha^*_{132}\,\alpha^*_{121}/\alpha^*_{123}\,\alpha_{112} + \alpha^*_{231}/\alpha^*_{123})$ are determined from equations (10) and (14) by minimizing $[E(t) - E(0)\,\mathrm{e}^{-2[\varepsilon\mu_1 t + g(\varepsilon t)]}]^2$. From equation (13) one can define two functions, $F_1(t) = \phi_1' a_1^2(t)$ and $F_2(t) = -A\phi_2' a_2^2(t) - B\phi_3' a_3^2(t)$ which, on a suitable time plot, should appear as "mirror images" once the values for A and B are obtained by minimizing $[F_1(t) + F_2(t)]^2$. A second value for $(\omega_2/\omega_1)(\alpha_{112}/\alpha^*_{121})$ is found from A, while a value for $(\omega_3/\omega_1)\{\alpha^*_{231}/\alpha^*_{123} - \alpha^*_{132}\,\alpha^*_{121}/\alpha^*_{123}\,\alpha_{112}\}$ can be obtained from B. As will be seen in the examples to follow, the matching of the mirror image functions $F_1(t)$ and $F_2(t)$ can be a very sensitive check on the correctness of the analyzing frequencies ω_n used in the STFT analysis.

Experimental data will normally be obtained or stored in discretized form as a result of sampling. The real functions $E(t)$ and $F_m(t)$ $(m = 1, 2)$ will be represented by the sequences

$$E_j, F_{m,j}, \qquad j = 0, \ldots, N-1,$$

where N represents the number of data points in the whole sample. The procedure therefore requires the minimization of the residuals

$$K_E = \frac{1}{N}\sum_{j=0}^{N-1}[E_j - E_0\,\mathrm{e}^{-2(\mathrm{j}\varepsilon\mu_1\,\delta t + g_j)}]^2, \qquad K_F = \frac{1}{N}\sum_{j=0}^{N-1}[F_{i,j} + F_{2,j}]^2, \tag{15a, b}$$

where δt is the sampling interval. Time derivatives of the phase are estimated using the phase change over successive discrete time samples.

2.3. SYNTHESIS

On completing the minimization procedure, the parameters and parameter ratios can be used to synthesize the steelpan response during the period of free vibrations (more precisely, from the instant that E maximizes to the end of the tone).

It was shown in Part I, that the tonal structure (frequency and amplitude) depends on the manner in which the stick impact is delivered. When the note is played with more

vigour, the level of the second mode increases significantly in comparison with the first mode. The note synthesis must therefore take this into account. Following the procedure adopted in Parts I and II, a note judged to have been played at the *forte* level (loud) can be simulated in the numerical experiments by assuming an initial amplitude for the first mode as $a_1(0) = 1$. Similarly, a note at the *piano* level (soft) will have $a_1(0) = 0{\cdot}5$.

The non-uniqueness of the α-parameters allows a wide range of values that may be acceptable in the synthesis. However, the α-ratio values determined in the minimization procedure must be satisfied. In addition, the time scale in the synthesis is arbitrary, but in this case it is necessary to keep the ratio of the detuning parameters consistent with the results obtained in the minimization procedure.

3. EXAMPLE APPLICATIONS

The algebraic simplicity of the results in the previous section allow for the straightforward application of the inverse procedure to the vibrations of the steelpan notes. Two examples are taken from the example set of Part I. The first example corresponds to a note for which there is a weak second mode and negligible higher modes, while in the second example there is a strong second mode and a comparatively weaker third mode. These examples are typical of those found on this instrument. Note excitation was done in the normal way for this instrument, by striking the note with the stick and velocity recordings are made in the manner described earlier for *observation data*.

Derivatives with respect to real time t replace derivatives with respect to τ, since the factor ε cancels out across equation (13). The sampling rate for the data was 11 kHz. Sampling faster produced no additional information. The procedures for setting the parameters for the Gaussian window and the variance in the STFT computations were the same as those used in Part I. For the synthesis of the steelpan responses, equations (3a–f) were integrated numerically using a fourth order Runge–Kutta routine which produced the discretized values for a_n and ϕ_n at time steps of 0·1.

Minimization of equation (15a) was first done assuming different decay coefficients and then by assuming equal decay coefficients with g_j set to zero. It was necessary to perform separate minimization for each case because of the non-linear nature of the problem.

3.1. THE $F_4^{\#}$ NOTE ON A TENOR PAN

The tone structure (modal components) for the $F_4^{\#}$ (369·99 Hz) note, played *forte*, is shown in Figure 1. This particular note shows a modulated first mode component and a weak, modulated, second mode. Higher modes were not present. Because of a small mistuning of this note at the time of the experiment, STFT's were maximized [1] at $f_1 = 367{\cdot}3$ Hz and $f_2 = 743{\cdot}2$ Hz for a frequency ratio $f_2/f_1\,(\omega_2/\omega_1) = 2{\cdot}0234$. The product $\varepsilon\sigma_1 = 54{\cdot}0$ rad/s $\equiv 8{\cdot}6$ Hz.

$E(t)$ reached a maximum some 13·8 ms after the stick struck this note. This time interval is approximately five times the period of the first mode. The minimization of the residual K_E yielded the values $\varepsilon\mu_1 = \varepsilon\mu_2 = 3{\cdot}17\ \mathrm{s}^{-1}$, $\alpha^*_{121}/\alpha_{112} = 53{\cdot}4$ under the equal damping assumption and $\varepsilon\mu_1 = 3.15\ \mathrm{s}^{-1}$, $\varepsilon\mu_2 = 3{\cdot}27\ \mathrm{s}^{-1}$; $\alpha^*_{121}/\alpha_{112} = 53{\cdot}4$ otherwise.

In Figure 2 the function $E(t)$ from equation (8) is seen closely to follow the exponential function $E(0)\,\mathrm{e}^{-2\varepsilon\mu t}$. In Figure 3 is shown the percentage deviation between $E(t)$ defined in equation (8) and $E(t)$ according to equation (10). This deviation is less than half of one percent for the first 0·55 s. At the end of this period $E(t)$ has already decayed to less than 4 percent of its initial value. It is therefore reasonable to conclude that there is no significant difference between the damping coefficients for the two modes on this note.

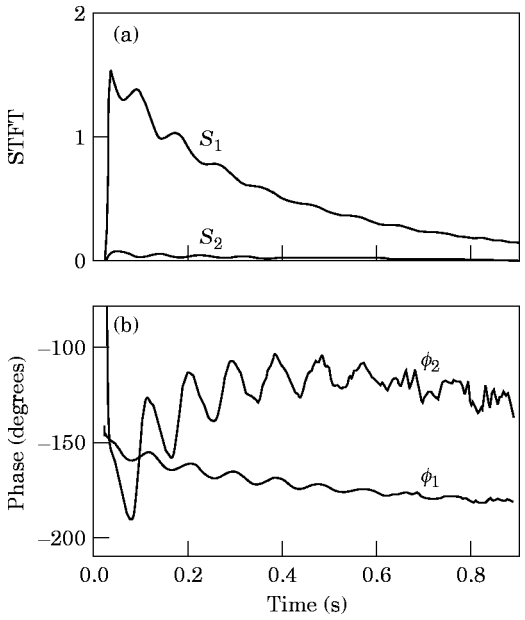

Figure 1. Observation data for the $F_4^\#$ note in the form of Fourier components: (a) the amplitudes $|S_n|$; (b) the phase angles arg (S_n).

Minimization of the residual K_F yielded the value $\alpha_{121}^*/\alpha_{112} = 44{\cdot}0$. This value is some 21 percent lower than that obtained by minimizing K_E. The mirror functions $F_1(t)$ and $F_2(t)$ are plotted in Figure 4. While adjustments to the value of A $(=(\omega_2/\omega_1)(\alpha_{112}/\alpha_{121}^*))$ in the minimization process will produce changes to the magnitude of the function $F_2(t)$, it will not alter the *form* of $F_2(t)$. There is a fair degree of detailed matching in the form of the functions $F_1(t)$ and $F_2(t)$ seen in Figure 4. This suggests that the analytical model can be applied with confidence to this musical instrument.

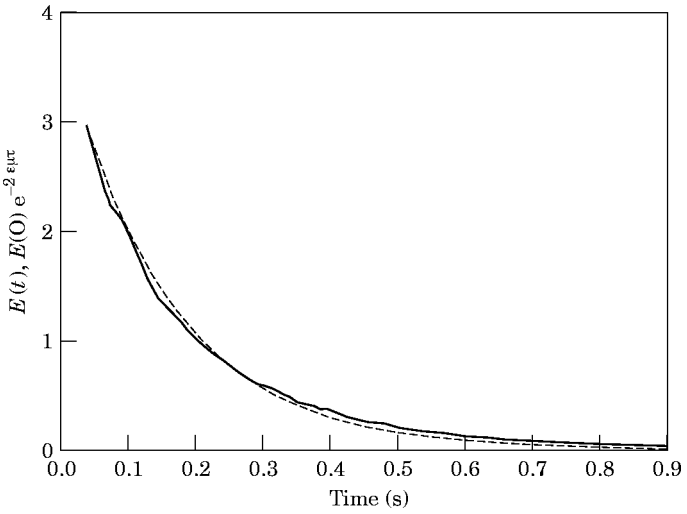

Figure 2. The functions $E(t)$ (—) and $E(0)e^{-2\varepsilon\mu t}$ (---) for the $F_4^\#$ note.

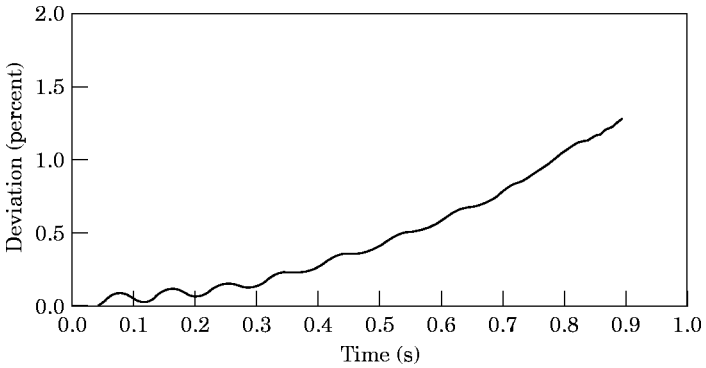

Figure 3. The percentage deviation between $E(t)$ defined by equation (8) and $E(t)$ defined by equation (10), for the $F_4^{\#}$ note.

3.2. $F_4^{\#}$ SYNTHESIS

The non-linear response of the $F_4^{\#}$ note was modelled numerically by integrating equations (3a, b, d, e) with the parameters $\alpha_{121}^{*} = 0{\cdot}16$, $\alpha_{112} = 0{\cdot}0033$, $\varepsilon\sigma_1 = 0{\cdot}01$, $\mu_1 = 0{\cdot}0006$ and $\mu_2 = 0{\cdot}00062$. The mean parameter ratio for $\alpha_{121}^{*}/\alpha_{112}$, obtained by minimization of the residuals, is satisfied by these α-parameters. To simulate the note played *forte*, the initial (dimensionless) displacement on the first mode was set at unity. The simulated amplitudes a_1 and a_2 are shown in Figure 5(a), while the corresponding phases ϕ_1 and ϕ_2 are shown in Figure 5(b). There is a marked similarity between the real note vibration data of Figure 1 and the simulated results in Figure 5.

3.3. THE E_4^{b} NOTE

A more complex tone structure is shown in Figure 6 for the E_4^{b} (311·1 Hz) note played *forte*. To determine these components, the STFT's were maximized with $f_1 = 311{\cdot}1$ Hz, $f_2 = 624{\cdot}0$ Hz and $f_3 = 930{\cdot}6$ Hz. The corresponding frequency ratios are $f_2/f_1 = 2{\cdot}006$ and $f_3/f_1 = 2{\cdot}991$ with $\varepsilon\sigma_1 \equiv 1{\cdot}8$ Hz and $\varepsilon\sigma_2 \equiv -4{\cdot}5$ Hz.

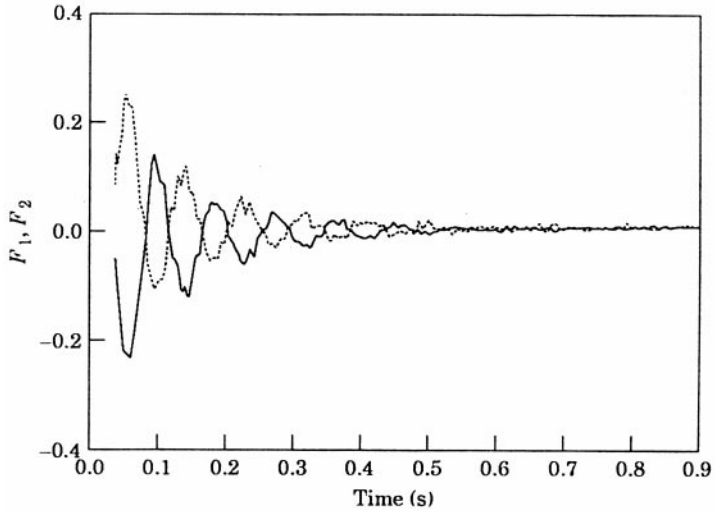

Figure 4. The mirror functions $F_1(t)$ (—) and $F_2(t)$ (· · · ·) for the $F_4^{\#}$ note.

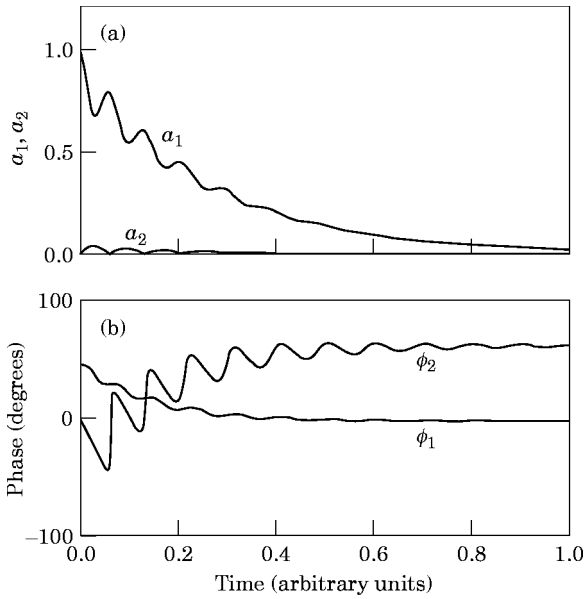

Figure 5. Numerical simulation of the $F_4^{\#}$ note: (a) amplitudes; (b) phase angles.

On this note, $E(t)$ reached a maximum 16·5 ms after the note was struck (approximately five times the period of the first mode). The minimization of the residual K_E yielded the values $\varepsilon\mu_n = 3{\cdot}53\ \mathrm{s}^{-1}$ $(n = 1, 2, 3)$, $\alpha_{121}^*/\alpha_{112} = 2{\cdot}89$ and $(\alpha_{231}^*/\alpha_{123}^* + \alpha_{132}^*\,\alpha_{121}^*/\alpha_{123}^*\,\alpha_{112}) = 1{\cdot}24$ under the equal damping assumption, and $\varepsilon\mu_1 = 3{\cdot}52\ \mathrm{s}^{-1}$, $\varepsilon\mu_2 = 3{\cdot}72\ \mathrm{s}^{-1}$, $\varepsilon\mu_3 = 3{\cdot}52\ \mathrm{s}^{-1}$, $\alpha_{121}^*/\alpha_{112} = 2{\cdot}89$ and $(\alpha_{231}^*/\alpha_{123}^* + \alpha_{132}^*\,\alpha_{121}^*/\alpha_{123}^*\,\alpha_{112}) = 1{\cdot}24$ otherwise (notice that both analyses yield the same α-ratios). In Figure 7, the function $E(t)$ from equation (8) is seen, for this note also, to closely follow the exponential function $E(0)\,\mathrm{e}^{-2\varepsilon\mu t}$.

The deviation between $E(t)$ defined by equation (8) for equal damping and $E(t)$ according to equation (10) is plotted in Figure 8. The absolute magnitude of this deviation remains less than 0·2 percent for the duration of the tone. Here also, it is clearly demonstrated that the equal damping assumption is applicable to the steelpan notes.

Minimizing the residual K_F yielded the values $\alpha_{121}^*/\alpha_{112} = 2{\cdot}49$ and $(\alpha_{231}^*/\alpha_{123}^* - \alpha_{132}^*\,\alpha_{121}^*/\alpha_{123}^*\,\alpha_{112}) = 0{\cdot}54$. As with the $F_4^{\#}$ note, the value for $\alpha_{121}^*/\alpha_{112}$ obtained by minimizing K_F is less than the value obtained by minimizing K_E, this time by 16 percent. Combining the two sets of results for the parameters, one also obtains the values $\alpha_{231}^*/\alpha_{123}^* = 0{\cdot}89$ and $\alpha_{132}^*/\alpha_{123}^* = 0{\cdot}14$ *or* 0·12 (the latter values corresponding to $\alpha_{121}^*/\alpha_{112} = 2{\cdot}49$ or 2·89).

In Figure 9, the mirror functions $F_1(t)$ and $F_2(t)$ are plotted along with the contribution $G_3(t) = -B\phi_3' a_3^2(t)$ (scaled up $\times 10$) by the third mode to $F_2(t)$. From Figure 9 it is clear that, in this example, it is the second mode that largely determines the form of the function $F_2(t)$.

3.4. E_4^b SYNTHESIS

The non-linear response of the E_4^b note was modelled numerically by integrating equations (3a–f) with the parameters $\alpha_{121}^* = 0{\cdot}047$, $\alpha_{112} = 0{\cdot}019$, $\alpha_{123}^* = 0{\cdot}007$, $\alpha_{231}^* = 0{\cdot}006$, $\alpha_{132}^* = 0{\cdot}0009$, $\mu_1 = 0{\cdot}00067$, $\mu_2 = 0{\cdot}00067$, $\mu_3 = 0{\cdot}00067$, $\varepsilon\sigma_1 = 0{\cdot}002$ and $\varepsilon\sigma_2 = -0{\cdot}0048$. The parameter ratios obtained by minimization of the residuals are satisfied by these parameters. To simulate the note played *forte*, the initial (dimensionless) displacement on the first mode was set at unity.

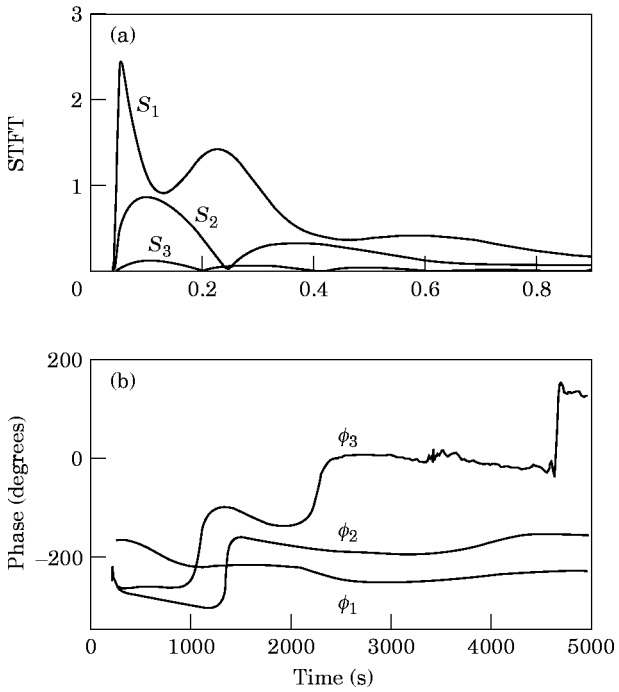

Figure 6. Observation data for the E_4^b note in the form of Fourier components: (a) the amplitudes $|S_n|$; (b) the phase angles arg (S_n).

The simulated amplitudes a_1 and a_2 are shown in Figure 10(a) (compare with Figure 6(a)) while the corresponding phases for ϕ_1 and ϕ_2 are shown in Figure 10(b) (compare with Figure 6(b)). Due to the small contribution of the third mode to $F_2(t)$, as noted earlier, the amplitude modulations on the simulated third mode did not closely match the corresponding structure on the real data. The most likely reason for this behaviour is the stronger contribution of cubic non-linearity to the third mode through internal resonance

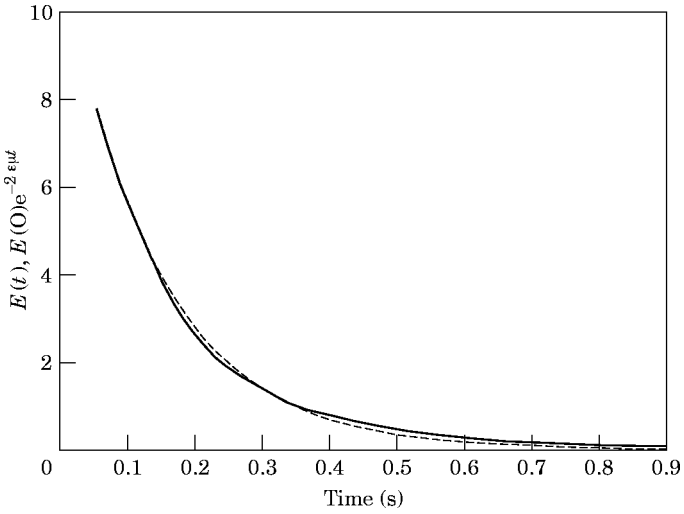

Figure 7. The functions $E(t)$ (—) and $E(0)e^{-2\varepsilon\mu t}$ (---) for the E_4^b note.

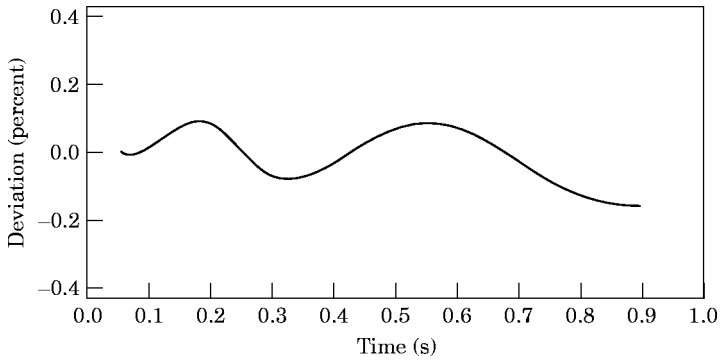

Figure 8. The percentage deviation between $E(t)$ defined by equation (8) and $E(t)$ defined by equation (10), for the E_4^b note.

than the contribution through combination resonance as assumed here. There are, however, strong similarities between the real and simulated amplitude and phase structures for the first two modes that dominated the dynamics of this note.

3.5. OPTIMIZING THE STFT

To demonstrate the sensitivity of the present method to changes in the analyzing frequency used in the STFT, the analyzing frequency for the second mode was reduced from the optimized value of $f_2 = 624{\cdot}0$ Hz to a new value of $623{\cdot}4$ Hz (a frequency reduction of just under $0{\cdot}1$ percent) and the Fourier component for the second mode was recalculated. With this being the only change to the analysis, the new results are shown in Figure 11. There is now no matching of the mirror functions $F_1(t)$ and $F_2(t)$. The form of $F_2(t)$ has changed completely. This change was brought about mainly by the phase component $\phi_2(t)$, as there were only very small changes to the amplitude $a_2(t)$. In addition to maximizing the STFT and minimizing the phase in the usual way [1], the matching of these two mirror functions serves as a sensitive check on the accuracy of the mode frequencies.

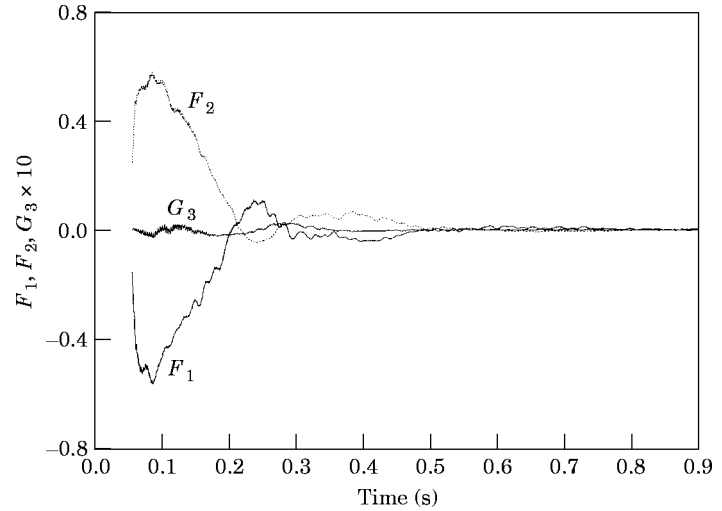

Figure 9. The functions $F_1(t)$, $F_2(t)$ and $G_3(t)$ for the E_4^b note with mode 2 maximized at $f_2 = 624{\cdot}0$ Hz.

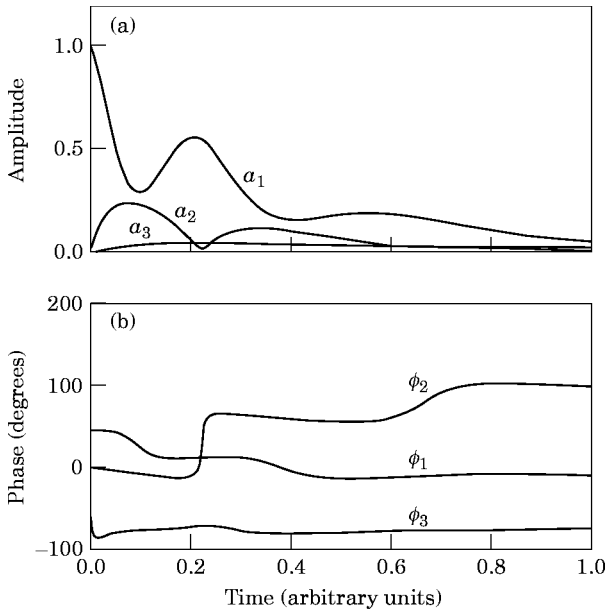

Figure 10. Numerical simulation of the E_4^b note: (a) amplitudes; (b) phase angles.

3.6. COMPARISON OF NOTE DYNAMICS

In comparing these two notes, one ought to look at the ratio $\alpha_{112}/\alpha_{121}^*$, for which the average value on the $F_4^\#$ note is 0·02, while on the E_4^b note it is 0·37. This shows that in both cases the coupling constant α_{112}, which is a measure of the coupling of mode 1 energy into mode 2, is less than α_{121}^*, which is a measure for the reverse coupling of energy from mode 2 back to mode 1. The process of energy exchange is, however, much more effective on the E_4^b note. This accounts for the more complex structure obtained on this E_4^b note and explains its much greater brilliance (musically).

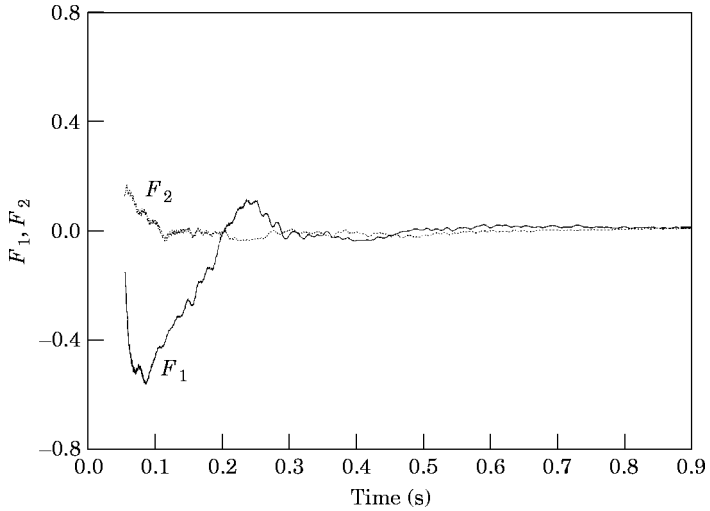

Figure 11. The functions $F_1(t)$ (—) and $F_2(t)$ (· · · ·) for the E_4^b note with mode 2 maximized at $f_2 = 623{\cdot}4$ Hz.

4. CONCLUSIONS

The model parameters for the non-linear vibrations of the notes on the steelpan as developed in the analysis of references [1] and [2] can be computed by the inverse process developed here. It was verified that approximately equal damping exists for all the modes on a note. Equal damping leads to the result that a weighted sum of the squares of the modal amplitude should follow an exponential decay law. This decay law was found to be closely obeyed on the two notes chosen as examples. Minimization procedures gave estimates for the decay coefficients and the weights from which the α-parameter ratios were computed. The synthesized tonal structures, using model parameters consistent with the analysis, closely matched the real data.

In essence, the computations are relatively simple. After computing the STFT for the tone signal (velocity or displacement time-history) the amplitude and phase data are used in the expressions for the residuals K_E and K_F which are then minimized. The matching of the two functions defining K_F plays the additional role of a very sensitive check on the accuracy of the analyzing frequencies used in the STFT computation.

REFERENCES

1. A. Achong 1996 *Journal of Sound and Vibration* **197**, 471–487. The steelpan as a system of non-linear mode-localized oscillators, part I: theory, simulations, experiments and bifurcations.
2. A. Achong and K. A. Sinanan-Singh 1997 *Journal of Sound and Vibration* **203**, 547–561. The steelpan as a system of non-linear mode-localized oscillators, part II: coupled sub-systems, simulations and experiments.
3. P. Lancaster and J. Maroulas 1987 *Journal of Mathematical Analysis and Applications* **123**, 238–261. Inverse eigenvalue problems for damped vibrating systems.
4. L. Starek and D. J. Inman 1992 *Transactions of the American Society of Mechanical Engineers*, *Journal of Vibration and Acoustics* **114**, 564–568. A symmetric inverse vibration problem.
5. L. Starek and D. J. Inman 1995 *Journal of Sound and Vibration* **181**, 893–903. A symmetric inverse vibration problem with overdamped modes.
6. G. M. L. Gladwell 1986 *Applied Mechanics Review* **39**, 1013–1018. Inverse problems in vibration.
7. G. M. L. Gladwell 1996 *Applied Mechanics Review* **49**, S25–S34. Inverse problems in vibration—II.
8. J. E. Mottershead and M. I. Friswell 1993 *Journal of Sound and Vibration* **167**, 347–375. Model updating in structural dynamics: a survey.
9. A. Achong 1996 *Journal of Sound and Vibration* **191**, 207–217. Vibrational analysis of mass loaded plates and shells by the receptance method with application to the steelpan.
10. A. H. Nayfeh and D. T. Mook 1979 *Nonlinear Oscillations*. New York: Wiley-Interscience.
11. A. H. Nayfeh 1983 *Journal of Sound and Vibration* **90**, 237–244. The response of multidegree-of-freedom systems with quadratic non-linearities to a harmonic parametric resonance.
12. P. R. Sethna 1965 *Transactions of the American Society of Mechanical Engineers*, *Journal of Applied Mechanics* **32**, 576–582. Vibrations of dynamical systems with quadratic nonlinearities.
13. C. M. Harris (editor) 1987 *Shock and Vibration Handbook*. New York: McGraw-Hill.